DELFT UNIVERSITY OF TECHNOLOGY, FACULTY OF AEROSPACE ENGINEERING

AE4301P: Automatic Flight Control System Design Assignment Report

Ward Bogaerts, student number: 5378273
Basem Deeb, student number: 5197368
Chari Loukisas, student number: 5185521
February 1, 2022

CONTENTS

1. Report introduction **4**

2. Trim and Linearisation **4**
2.1. Simulink model adjustment . . . 4
2.2. Linearization and cost function . . . 4
2.3. Trimming and linearisation results and accuracy . . . 4
2.3.1. Evaluation of result reliability . . . 5
2.4. Accelerometer inclusion . . . 6
2.5. Accelerometer response initial analysis . . . 7
2.5.1. Negative step response analysis . . . 7
2.5.2. Initial discussion . . . 8
2.6. Analysis of changing x_a . . . 9
2.7. Further analysis of results . . . 11

3. Open loop analysis **11**
3.1. Trimming and linearization . . . 11
3.2. Determination of reduced state-space model . . . 11
3.2.1. 6x6 state space with actuator dynamics included . . . 11
3.2.2. 4x4 Longitudinal model . . . 12
3.2.3. 4x4 Lateral model . . . 13
3.3. Calculation of inherent motion characteristics . . . 13
3.3.1. Time responses periodic eigenmotions . . . 13
3.3.2. Time responses of aperiodic eigenmotions . . . 14

4. Design of a pitch rate command system **15**
4.1. Short period reduced model . . . 15
4.2. Requirements of the CAP and Gibson criteria and pole placement . . . 18
4.3. Lead-Lag filter . . . 19
4.4. Verification of CAP and Gibson criteria . . . 19
4.5. Gain Scheduling . . . 21

5. Design of automatic glideslope following and flare controller **21**
5.1. Trimming and linearisation . . . 21
5.2. Reduced model . . . 22
5.3. Aircraft model . . . 22
5.4. Airfield module and glide slope controller . . . 23
5.4.1. Airfield: Glide slope error angle and slant range . . . 23
5.4.2. Glide slope controller . . . 24
5.5. Flare controller . . . 25

A. Aircraft Simulink model **27**

B. Flare Controller Simulink model **28**

C. Airfield module **29**

D. Glide slope coupler **30**

E. Complete system **31**

List of Figures

2.1. Adjusted Simulink model with a_n (Short period) . . . 5
2.2. Accelerometer long-term response to a negative step elevator input . . . 7
2.3. Accelerometer initial response to a negative step elevator input . . . 8
2.4. Pole-zero map indicating zeros on the right half plane . . . 9
2.5. Different responses for different x_a values . . . 10
2.6. Different responses for different x_a values (zoomed) . . . 10
3.1. Pitch rate step response to elevator input (Short period) . . . 14
3.2. Pitch attitude response to elevator step input (Phugoid) . . . 15
3.3. Response of sideslip angle, roll angle, roll rate and yaw rate to rudder impulse input (Dutch roll) . . . 15
3.4. Roll angle impulse response to aileron (Spiral) . . . 16
3.5. Roll rate response to aileron step input (Aperiodic roll) . . . 16
4.1. Pitch rate q response on a step input for 2 states and 4 states . . . 17
4.2. Pitch rate q response on a step input for 2 states and 4 states, longer time . . . 17
4.3. Pitch rate tracking response to a step input . . . 20
4.4. Pitch angle tracking response to a step input . . . 20
4.5. Criterion for the tracking response for the reduced model . . . 21
4.6. Criterion for the tracking response for the reduced model using interpolation . . . 22
5.1. Graphical representation of the glide slope . . . 23
5.2. Aircraft path relative to airport altitude . . . 24
5.3. Flare Controller Geometry . . . 25
5.4. Flare manoeuvre . . . 25

List of Tables

2.1. Used flight conditions . . . 4
2.2. Cost function values after trimming . . . 5
2.3. Cost function values for trimming iterations . . . 5
2.4. Zeros for different x_a values . . . 11
3.1. Poles, damping and natural frequency for the reduced longitudinal model . . . 13
3.2. Poles, damping and natural frequency for the reduced lateral model . . . 14
5.1. Tuning values cor aircraft control loops . . . 23

1. Report introduction

This practical is a follow-up course for the Automatic Flight Control System Design. The objective of the report is to design two command systems for F16, which are pitch rate command system and a terrain following system. Classical control theory has been used in the making of the control systems.

2. Trim and Linearisation

Linearisation is done in order to easily model and predict system behaviour. As by definition the linearised model is a linear approximation, it is crucial the system threshold is not exceeded for which the error of a linear approximation and the actual system dynamics is sufficiently small.
In this context, trimming the aircraft will result in a steady-state flight condition, for which relatively small deviations (due to e.g. a disturbance) can be approximated using a linearised system. If the flight condition would not be steady-state, the aircraft states would soon be dominated by heavily non-linear dynamics, defying the purposes of the analysis. For this reason, trimming before linearising the model is necessary.

The F-16 model was trimmed and linearised for 4 flight conditions: For these conditions, both the

Flight condition	Airspeed [ft/s]	Altitude [ft]	Attitude
1	500	15000	Level flight, straight wings
2	900	20000	Level flight, straight wings
3	600	20000	Level flight, straight wings
4	300	5000	Level flight, straight wings

Table 2.1: Used flight conditions

low-and high-fidelity models were trimmed and linearised using the **findF16Dynamics** function. The first flight condition is used to determine the influence of accelerometer position on the aicraft respones, the others are used for controller design.

2.1. Simulink model adjustment

In order to include the normal acceleration (including transport acceleration), the Simulink model has been adjusted in order to have a_n as an additional output. The normal acceleration is given by :

$$a_n = \frac{-(a_z - \dot{q}x_a)}{g_D} = n_z + \frac{\dot{q}x_a}{g_D} \tag{2.1}$$

Note that a positive acceleration is defined as "upwards" in reference to the aircraft body. In the "LIN F16Block" file, a link was made originating from the to be integrated F-16 states, as depicted in figure 2.1.

2.2. Linearization and cost function

In order to linearise the the low fidelity model, iterations have to be made until a steady state has been reached. To determine the accuracy of this steady state for modelling purposes, the cost function has been defined: $cost = 5\dot{h}^2 + W_\phi\dot{\phi}^2 + W_\theta\dot{\theta}^2 + W_\psi\dot{\psi}^2 + 2\dot{v_{tot}}^2 + 10\dot{\alpha}^2 + 10\dot{\beta}^2 + 10\dot{p}^2 + 10\dot{q}^2 + 10\dot{r}^2$. This function should be minimised to ensure an accurate linear description of the model. It is clear that the cost function takes into account angular (and altitude) rates and sums these rates.

2.3. Trimming and linearisation results and accuracy

By inputting the flight conditions listed in table 2.1 into **findF16Dynamics**, the trimmed models for all conditions were obtained with associated trimming costs depicted in table 2.2

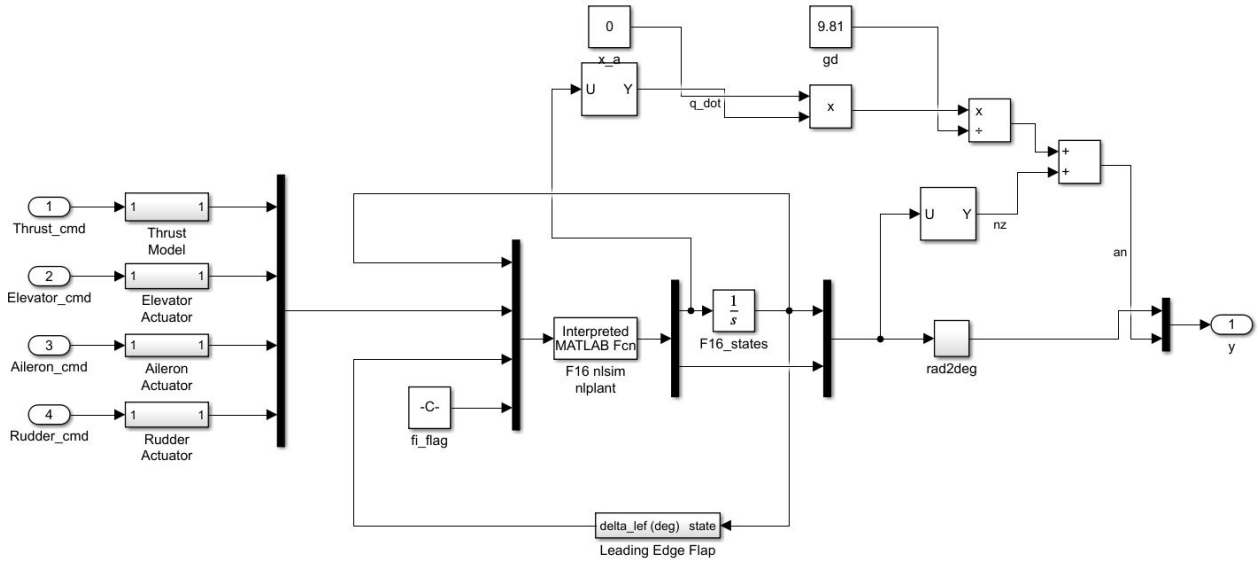

Figure 2.1: Adjusted Simulink model with a_n (Short period)

Flight condition 1		Flight condition 2		Flight condition 3		Flight condition 4	
High-fidelity	Low-fidelity	High-fidelity	Low-fidelity	High-fidelity	Low-fidelity	High-fidelity	Low-fidelity
7.1856e-06	4.2881e-29	9.1365e-07	2.2568e-26	4.4774e-06	4.9829e-29	7.8918e-06	4.7464e-30

Table 2.2: Cost function values after trimming

2.3.1. Evaluation of result reliability

The evaluation of result reliability is done for the low-fidelity model for flight condition 1, but the reasoning is analogous for other flight conditions and the high-fidelity models.

As can be seen in table 2.3, the initial cost values are extremely small. Even though this is the case, the optimum accuracy of the model is reached when the cost function does not change with more iterations. The values of the cost function per iteration:

Iteration	Cost function
1	5.5386e-29
2	5.444e-29
3	5.3486e-29
..	..
17	4.2976e-29
18	4.2881e-29
19	4.2881e-29

Table 2.3: Cost function values for trimming iterations

As a clear optimum is reached at iteration 18, and because the values of the cost function are negligibly small for short-time period analysis purposes, the model can be assumed to be accurate enough for the modelling purposes discussed in this report. Furthermore, the orders of magnitude obtained in table 2.2 correspond well to the the provided trimming/linearisation examples in the manual.
In general, the cost for linearising the low-fidelity models is around 20 orders of magnitude smaller than the high-fidelity trimming cost. This could be due to the HIFI model being more nonlinear and interdepenent than the LOFI model.

2.4. ACCELEROMETER INCLUSION

The accelerometer position is crucial in order to get accurate acceleration readings, especially when it is used for control purposes. This section aims to analyse different accelerometer placements and its effects. The analyses performed are done using the trimmed and linearised model of the low-fidelity F-16 model in flight condition 1.

Note that initially, x_a from equation 2.1 is taken to be zero (which translates to the accelerometer being placed on the centre of gravity, also the centre of rotation). This resulted in the following output vector:

$$y = \begin{bmatrix} n_{pos} & e_{pos} & h & \phi & \theta & \psi & V & \alpha & \beta & p & q & r & n_x & n_y & n_z & M & \bar{q} & p_s & a_n \end{bmatrix}^T \tag{2.2}$$

With a zero-valued D-matrix. Using this system definition of the form:

$$\dot{\bar{x}} = A\bar{x} + Bu \tag{2.3}$$

$$\dot{\bar{y}} = C\bar{x} + Du \tag{2.4}$$

the C-matrix gives the normal acceleration, given by the following equation of states:

$$a_n = -3.2432 * 10^{-5} * h - 9.679710^{-6} * \theta + 0.004 * V_t + 9.9298 * \alpha + 0.9664 * q + 0.0208 * n_y \tag{2.5}$$

The minimum elevator-to-normal-acceleration transfer function realisation can be extracted from this system:

$$\frac{a_n}{\delta_e} = \frac{0.421s^4 - 1.84s^3 - 22.15s^2 + 0.077s + 0.001231}{s^5 + 32.73s^4 + 33s^3 + 41.48s^2 + 0.5546s + 0.293} \tag{2.6}$$

2.5. Accelerometer response initial analysis

Now that the $\frac{a_n}{\delta_e}$ transfer function has been determined, the effects of different accelerometer placements (varying x_a) can be determined by means of step inputs.

2.5.1. Negative step response analysis

The long-time response to a negative elevator input (stick up, elevator deflected upwards):

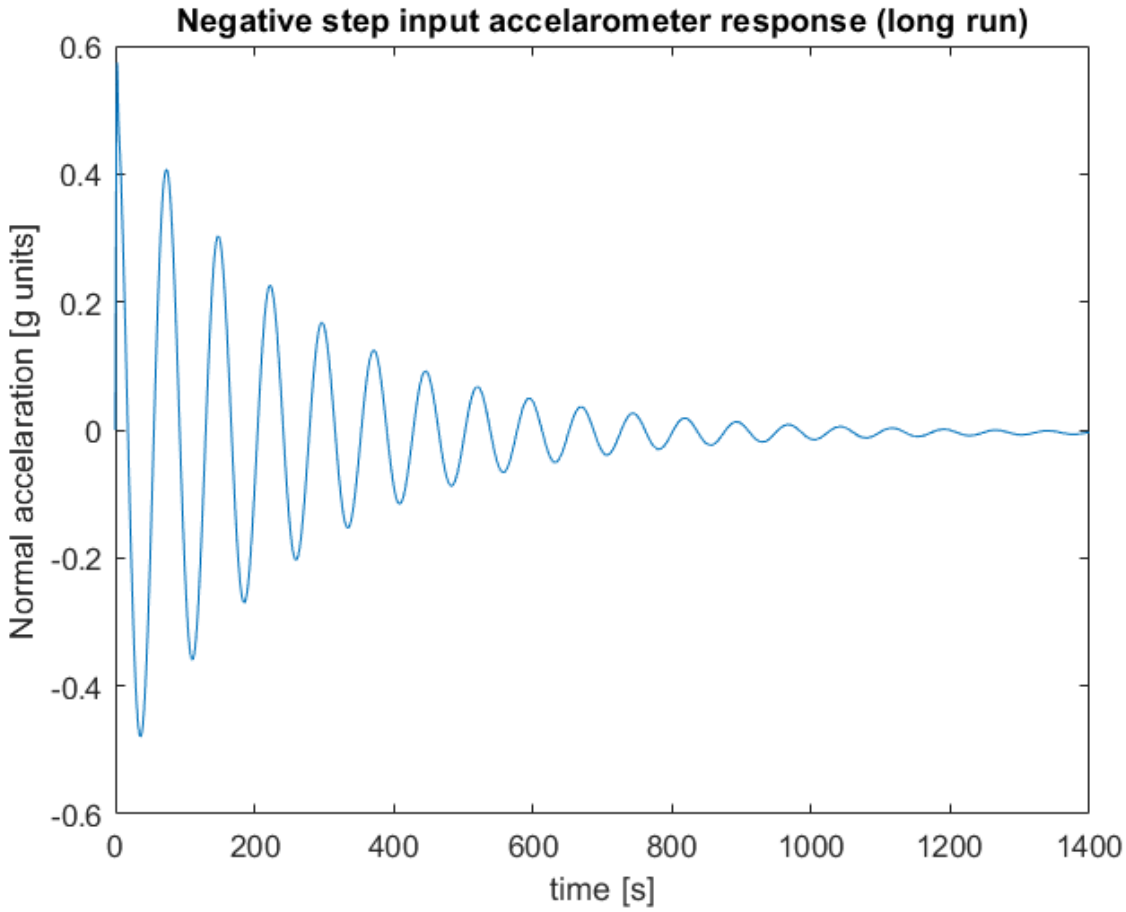

Figure 2.2: Accelerometer long-term response to a negative step elevator input

As can be expected, the short-period oscillation slowly dies out as the linearized aircraft model finds a new steady state. However, it is to be noted that the initial response of the aircraft clearly heads into the **opposite** (negative) direction of its stronger positive response afterwards (interval 0<t<0.2 seconds):

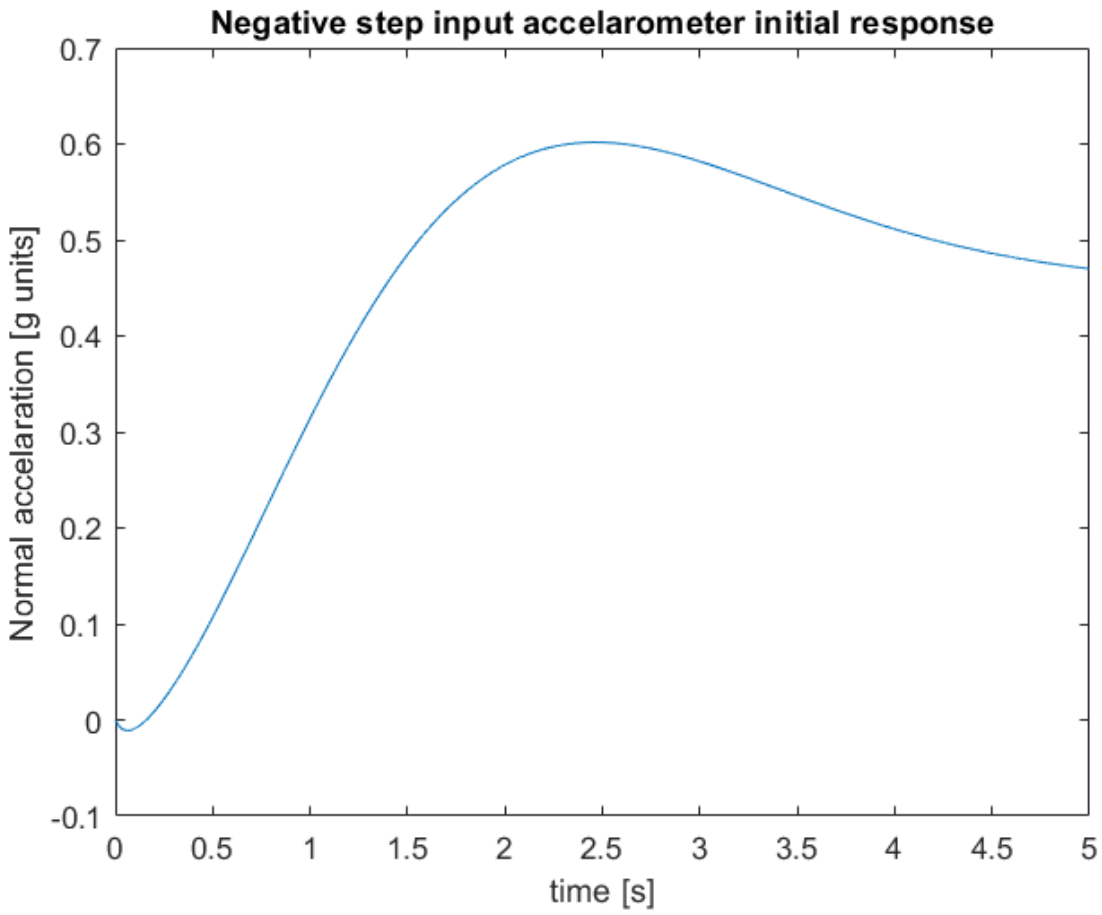

Figure 2.3: Accelerometer initial response to a negative step elevator input

2.5.2. INITIAL DISCUSSION

Analytically, the initial inverse response can be explained by presence of zeros in the (far) right half plane. This can be seen form the pole-zero map of the $\frac{a_n}{\delta_e}$ transfer function ($x_a = 0$):

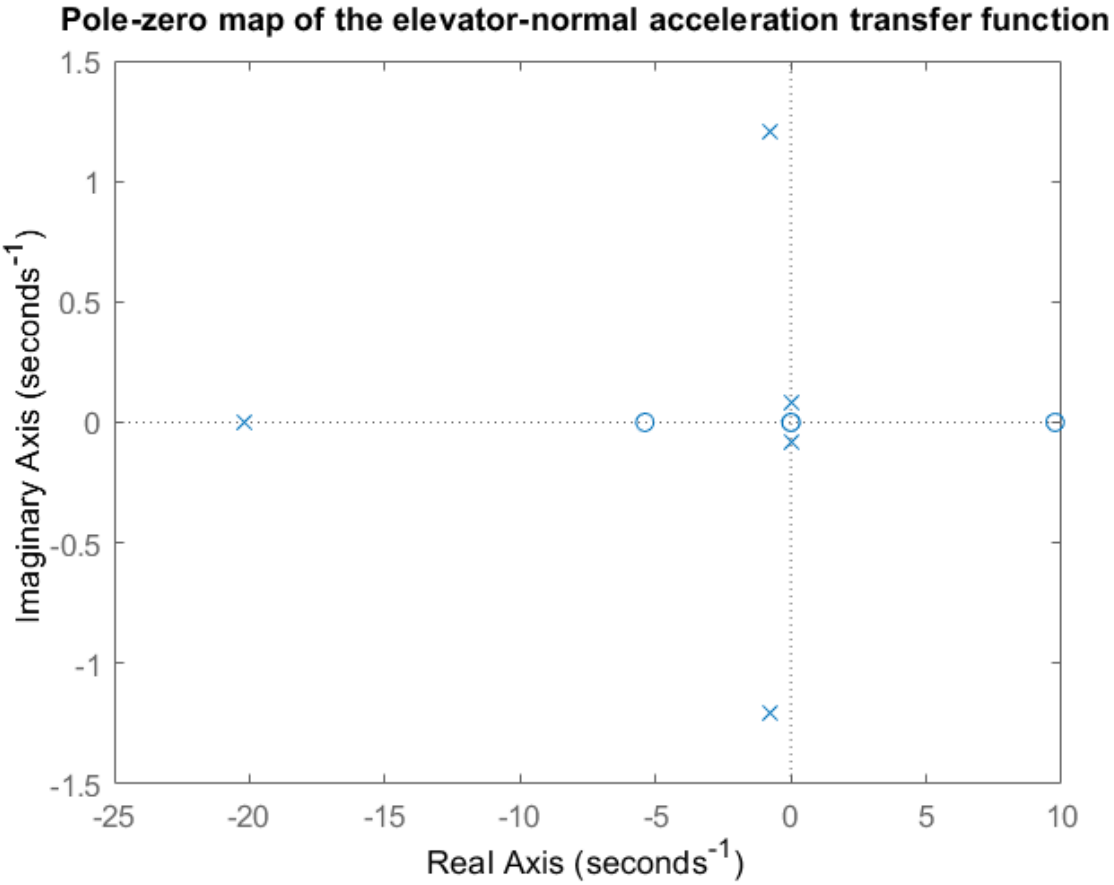

Figure 2.4: Pole-zero map indicating zeros on the right half plane

The zeros of which correspond to 9.7597, -5.3925, 0.0094 and -0.0059. These values are by definition the values for which the numerator of the $\frac{a_n}{\delta_e}$ transfer function becomes zero.
From a physical perspective, it can be seen from the negative step input graph that the accelerometer senses a downwards acceleration initially, after which it senses an acceleration upwards. This latter is logical in the sense that an upwards elevator deflection eventually results in a higher angle of attack, which in turn leads to an acceleration upwards due to the higher lift production. There is no rotational component in this measured acceleration, as x_a is zero, thus the location of the accelerometer is located on the centre of rotation. The initial inverse response can be explained by the fact that due to the upwards deflection, there is an instantaneous loss of lift leading to an acceleration "downwards". Rotating the F-16's angle of attack involves overcoming its inertia, which takes time. This is combined with the aerodynamics that also need to "catch up", resulting in a gradual increase in lift. Therefore, although in the long-run the increase in lift effect is dominant, it takes a longer time to take place than the faster loss of lift effect initially. This explains the initial inverse response.

2.6. Analysis of changing x_a

The behaviour of the accelerometer changes when x_a changes. The initial response is different due to the fact that rotational acceleration effects of the aircraft are included when $x_a \neq 0$ ft. Six values have been tested and are compared: $x_a = 0, 5, 5.9, 6, 7$ and 15 ft:

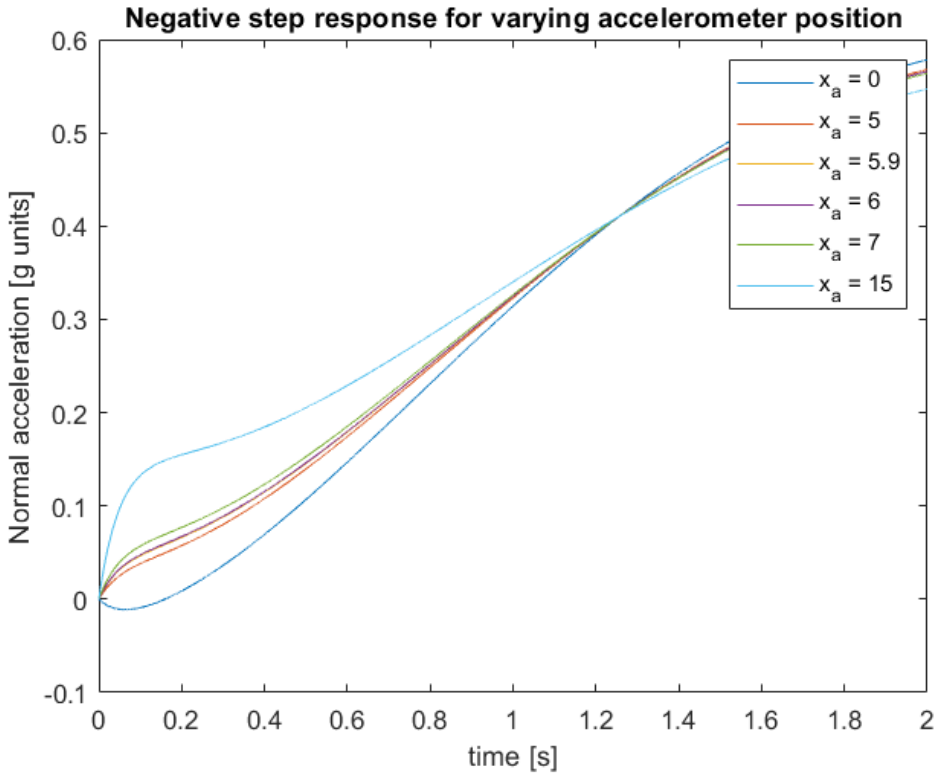

Figure 2.5: Different responses for different x_a values

Note that the values for $x_a = 5.9$ and $x_a = 6$ are graphically almost indistinguishable. For clarity, the graph zoomed in:

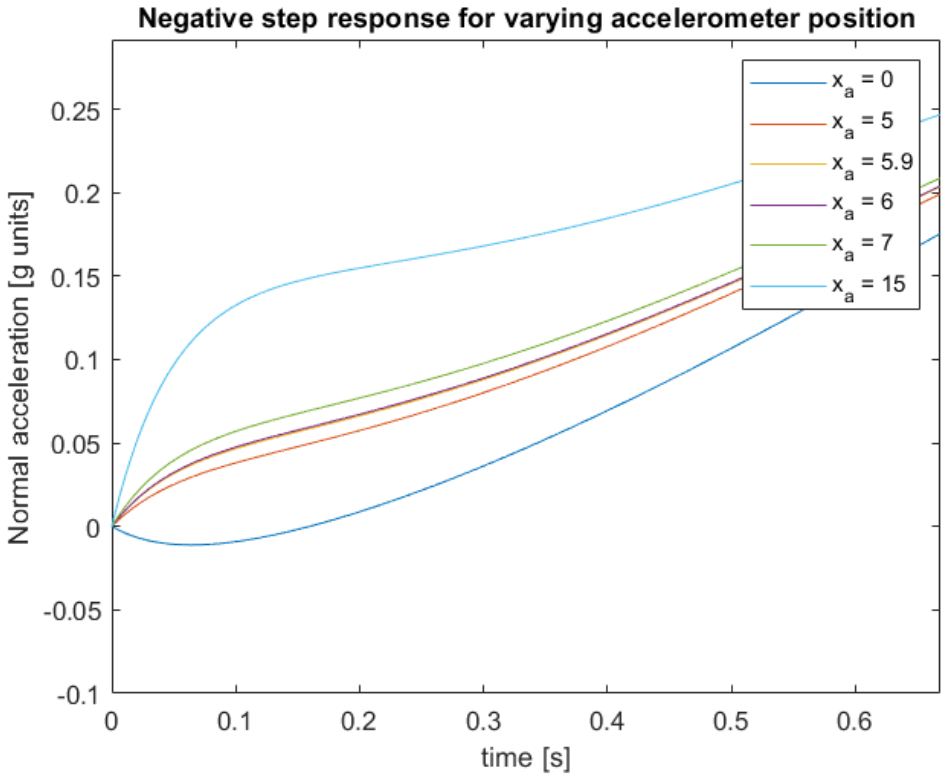

Figure 2.6: Different responses for different x_a values (zoomed)

The zeros of the x_a values are summarised in the table below. Note the (far) right half plane zeros are not existent anymore for the positive overshoot x_a values:

x_a [ft]	zeros	common zeros
0	9.7597; -5.3925	0.0094; -0.0059
5	-1.7251 ± 5.1587i	0.0094; -0.0059
5.9	-1.4165 ± 4.5924i	0.0094; -0.0059
6	-1.3904 ± 4.5403i	0.0094; -0.0059
7	-1.1844 ± 4.1002i	0.0094; -0.0059
15	-0.6599 ± 2.5974i	0.0094; -0.0059

Table 2.4: Zeros for different x_a values

The instantaneous centre of rotation is located where the net change in position due to the lowering in altitude combined with the translation of that location due to the rotation of the aircraft is equal to zero. Graphically this can be seen in the accelerometer measurements as having an initial response equal to zero in the same time interval where accelerometer readings of other positions show readings unequal to zero, after which the "dominating" lift change effect is felt. It is clear that the instantaneous centre of rotation is located on x_a values between 0 and 5 feet, as can be derived from figure 2.6

2.7. Further analysis of results

The cockpit is ideally placed in the location of the instantaneous centre of rotation. The reason for this is that this mitigates movements of the pilot to a minimum, which is important in high-performance combat aircraft due to the conditions both aircraft and pilot are exposed to. Next to this, the pilot will receive a minimum of "confusing" exposures, such as inverse initial-responses.
From the analyses of this chapter, it can also be concluded that the accelerometer needs to be placed close to a node of the most important fuselage bending mode. This is to prevent false readings due to fuselage bending under high aerodynamic loads.

3. Open loop analysis

3.1. Trimming and linearization

The low-fidelity model for flight condition 1 (table 2.1) was used.

3.2. Determination of reduced state-space model

The reduced state space model is obtained by first reducing the complete longitudinal and lateral LOFI state space models into two 6x6 state space models with actuator dynamics included. These are then reduced to the familiar 4x4 flight dynamics models.

3.2.1. 6x6 state space with actuator dynamics included

Longitudinal model
The 6x6 state space system was obtained by selecting the appropriate rows/columns for the following states: $\theta, V_t, \alpha, q, \delta_{el}, \delta_{th}$ and input signals: u_{el}, u_{eng}, which resulted in the following open loop longitudinal state

space system:

$$\dot{x}_{ol_{lon}} = \begin{pmatrix} 0 & 0 & 0 & 1.0 & 0 & 0 \\ -32.17 & -0.012198 & 37.063 & 0.14129 & 0.0015699 & 0.35493 \\ 1.1526e-13 & -0.000079265 & -0.97484 & 0.9505 & -2.1539e-8 & -0.0020498 \\ 0 & 1.8148e-17 & -4.2764 & -1.3174 & 0 & -0.3139 \\ 0 & 0 & 0 & 0 & -1.0 & 0 \\ 0 & 0 & 0 & 0 & 0 & -20.2 \end{pmatrix} \cdot \begin{pmatrix} \theta \\ V_t \\ \alpha \\ q \\ \theta_{el} \\ \theta_{th} \end{pmatrix}$$

$$+ \begin{pmatrix} 0 & 0 \\ 0 & 0 \\ 0 & 0 \\ 0 & 0 \\ 1.0 & 0 \\ 0 & 20.2 \end{pmatrix} \cdot \begin{pmatrix} u_{el} \\ u_{eng} \end{pmatrix}$$

$$y_{ol_{lon}} = \begin{pmatrix} 57.296 & 0 & 0 & 0 & 0 & 0 \\ 0 & 1.0 & 0 & 0 & 0 & 0 \\ 0 & 0 & 57.296 & 0 & 0 & 0 \\ 0 & 0 & 0 & 57.296 & 0 & 0 \end{pmatrix} \cdot \begin{pmatrix} \theta \\ V_t \\ \alpha \\ q \\ \theta_{el} \\ \theta_{th} \end{pmatrix} + \begin{pmatrix} 0 & 0 \\ 0 & 0 \\ 0 & 0 \\ 0 & 0 \end{pmatrix} \cdot \begin{pmatrix} u_{el} \\ u_{eng} \end{pmatrix}$$

Lateral model

Again, the 6x6 model is obtained by selecting the approriate rows and columns from the complete LOFI lateral state space model. For the lateral case, the 6 states are: $\beta, \phi, p, r, \delta_{ail}, \delta_{rud}$, with inputs: u_{ail}, u_{rud}. This results in the following 6x6 state space model:

$$\dot{x}_{ol_{lat}} = \begin{pmatrix} -0.30831 & 0.035742 & 0.011693 & -0.99594 & 0.00026279 & 0.00077128 \\ 0 & 0 & 1.0 & 0.012348 & 0 & 0 \\ -46.162 & 0 & -3.5711 & 0.51987 & -1.2187 & 0.20497 \\ 16.111 & 0 & 0.00027046 & -0.47572 & -0.076366 & -0.12788 \\ 0 & 0 & 0 & 0 & -20.2 & 0 \\ 0 & 0 & 0 & 0 & 0 & -20.2 \end{pmatrix} \cdot \begin{pmatrix} \beta \\ \phi \\ p \\ r \\ \delta_{ail} \\ \delta_{rud} \end{pmatrix}$$

$$+ \begin{pmatrix} 0 & 0 \\ 0 & 0 \\ 0 & 0 \\ 0 & 0 \\ 20.2 & 0 \\ 0 & 20.2 \end{pmatrix} \cdot \begin{pmatrix} u_{ail} \\ u_{rud} \end{pmatrix}$$

$$y_{ol_{lat}} = \begin{pmatrix} 57.296 & 0 & 0 & 0 & 0 & 0 \\ 0 & 57.296 & 0 & 0 & 0 & 0 \\ 0 & 0 & 57.296 & 0 & 0 & 0 \\ 0 & 0 & 0 & 57.296 & 0 & 0 \end{pmatrix} \cdot \begin{pmatrix} \beta \\ \phi \\ p \\ r \\ \delta_{ail} \\ \delta_{rud} \end{pmatrix} + \begin{pmatrix} 0 & 0 \\ 0 & 0 \\ 0 & 0 \\ 0 & 0 \end{pmatrix} \cdot \begin{pmatrix} u_{ail} \\ u_{rud} \end{pmatrix}$$

3.2.2. 4x4 Longitudinal model

The 4x4 longitudinal state space systems is obtained by selecting the appropriate rows/columns from the 6x6 state space system according to the method described in the assignment description. The resulting

state space matrices are depicted below:

$$\dot{x}_{lon} = \begin{pmatrix} 0 & 0 & 0 & 1.0 \\ -32.17 & -0.012198 & 37.063 & 0.14129 \\ 1.1526e-13 & -0.000079265 & -0.97484 & 0.9505 \\ 0 & 1.8148e-17 & -4.2764 & -1.3174 \end{pmatrix} \cdot \begin{pmatrix} \theta \\ V_t \\ \alpha \\ q \end{pmatrix} + \begin{pmatrix} 0 & 0 \\ 0.0015699 & 0.35493 \\ -2.1539e-8 & -0.0020498 \\ 0 & -0.3139 \end{pmatrix} \cdot \begin{pmatrix} \delta_{el} \\ \delta_{th} \end{pmatrix} \tag{3.1}$$

$$y_{lon} = \begin{pmatrix} 57.296 & 0 & 0 & 0 \\ 0 & 1.0 & 0 & 0 \\ 0 & 0 & 57.296 & 0 \\ 0 & 0 & 0 & 57.296 \end{pmatrix} \cdot \begin{pmatrix} \theta \\ V_t \\ \alpha \\ q \end{pmatrix} + \begin{pmatrix} 0 & 0 \\ 0 & 0 \\ 0 & 0 \\ 0 & 0 \end{pmatrix} \cdot \begin{pmatrix} \delta_{el} \\ \delta_{th} \end{pmatrix} \tag{3.2}$$

(3.3)

3.2.3. 4x4 Lateral model

The same method was used to determine the 4x4 lateral state space model:

$$\dot{x}_{lat} = \begin{pmatrix} -0.30831 & 0.035742 & 0.011693 & -0.99594 \\ 0 & 0 & 1.0 & 0.012348 \\ -46.162 & 0 & -3.5711 & 0.51987 \\ 16.111 & 0 & 0.00027046 & -0.47572 \end{pmatrix} \cdot \begin{pmatrix} \beta \\ \phi \\ p \\ r \end{pmatrix} + \begin{pmatrix} 0.00026279 & 0.00077128 \\ 0 & 0 \\ -1.2187 & 0.20497 \\ -0.076366 & -0.12788 \end{pmatrix} \cdot \begin{pmatrix} \delta_{ail} \\ \delta_{rud} \end{pmatrix} \tag{3.4}$$

$$y_{lat} = \begin{pmatrix} 57.296 & 0 & 0 & 0 \\ 0 & 57.296 & 0 & 0 \\ 0 & 0 & 57.296 & 0 \\ 0 & 0 & 0 & 57.296 \end{pmatrix} \cdot \begin{pmatrix} \beta \\ \phi \\ p \\ r \end{pmatrix} + \begin{pmatrix} 0 & 0 \\ 0 & 0 \\ 0 & 0 \\ 0 & 0 \end{pmatrix} \cdot \begin{pmatrix} \delta_{ail} \\ \delta_{rud} \end{pmatrix} \tag{3.5}$$

3.3. Calculation of inherent motion characteristics

First, the poles of the reduced longitudinal and lateral models have to be determined. These poles provide the necessary info to calculate the motion characteristics.

MATLAB provides a function to directly calculate the damping, natural frequency and the time constant for these poles using the *damp()* function. The period P and time to half amplitude $T_{\frac{1}{2}}$ can be calculated according to equations 3.6 and 3.7. The results are depicted in tables 3.1 and 3.2 for the longitudinal respectively lateral models.

$$P = \frac{2\pi}{\omega_d} = \frac{2\pi}{\omega_n \sqrt{1-\zeta^2}} \tag{3.6}$$

$$T_{\frac{1}{2}} = \frac{ln(2)}{\zeta \omega_n} \tag{3.7}$$

longitudinal poles	name	ζ [-]	ω_n [rad/s]	P [s]	$T_{\frac{1}{2}}$ [s]
-0.00602 ± 0.04470i	phugoid	0.133	0.0451	140.57	115.56
-1.15000 ± 2.01000i	short period	0.496	2.31	3.13	0.60

Table 3.1: Poles, damping and natural frequency for the reduced longitudinal model

3.3.1. Time responses periodic eigenmotions

Short period motion

The short period eigenmotion can be seen in the response of the pitch rate to an elevator step input on a short time scale, which is depicted in figure 3.1 for a response time of 15s. On the figure, 2 points

lateral poles	name	ζ [-]	ω_n [rad/s]	τ [s]	P [s]	$T_{\frac{1}{2}}$
-0.00774e ± 0.0000i	spiral	1	0.00774	129	/	89.55
-3.56000 ± 0.0000i	aperiodic roll	1	3.56	0.281	/	0.19
-0.39300 ± 4.07000i	Dutch roll	0.0962	4.09	/	1.54	1.76

Table 3.2: Poles, damping and natural frequency for the reduced lateral model

approximating 1 period are depicted as well. From these points it can be seen that the calculated period of 3.13s corresponds to the actual period of the response.

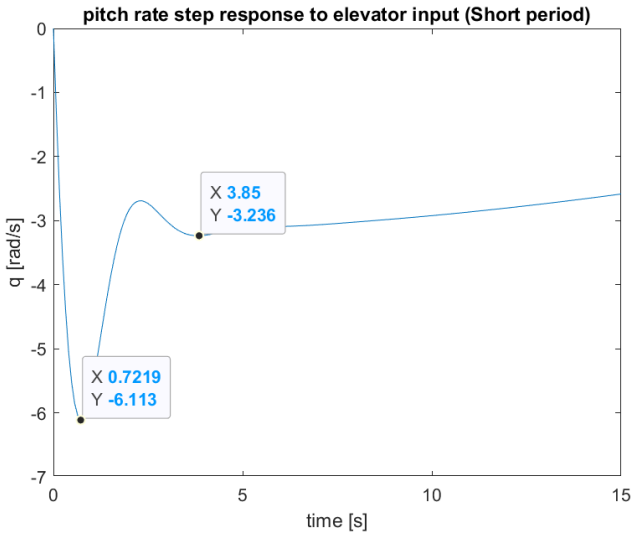

Figure 3.1: Pitch rate step response to elevator input (Short period)

Phugoid motion
The phugoid eigenmotion can be seen in the response of the pitch attitude θ to an elevator step input. This time, the observed time scale has to be larger than the one for the short period motions since the phugoid motion is a slow eigenmotion. Once again a point approximating 1 period of the eigenmotion are plotted in the figure to verify the calculated period, depicted in figure 3.2.

Dutch roll
The Dutch roll eigenmotion can be visualised by providing a rudder impulse to the system and observing the responses of the the sideslip angle β, the roll angle ϕ, the roll rate p and the yaw rate r. The results are shown in figure 3.3. In the figure, the calculated period can again be verified using the 2 indicated points.

3.3.2. Time responses of aperiodic eigenmotions

Spiral motion
The spiral eigenmotion describes roll stability. It can be visualised by plotting the impulse response of the roll angle to aileron input, as seen in figure 3.4. If unstable, the roll angle will keep on increasing. since the spiral pole is negative, the spiral mode will be stable. this can also be seen in figure , where the time to half amplitude is indicated as well and corresponds to the value obtained in table 3.2.

Aperiodic roll
The aperiodic roll eigenmotion can be visualised by plotting the roll rate response to an aileron step input, as shown in figure 3.5. This eigenmotion is very fast and damps out quickly, after which the response is dominated by the Dutch roll.

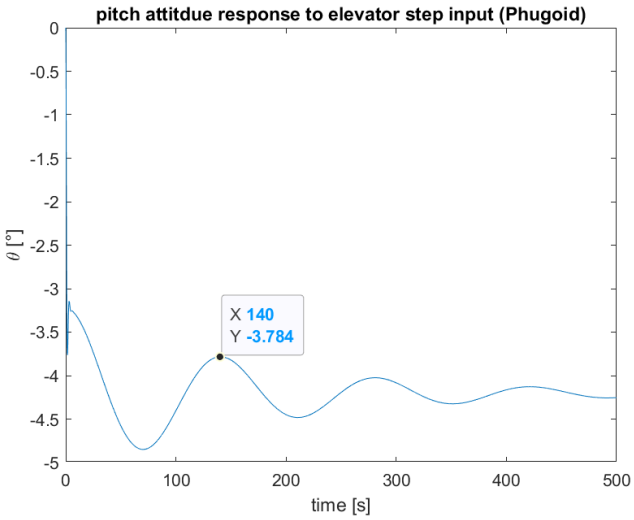

Figure 3.2: Pitch attitude response to elevator step input (Phugoid)

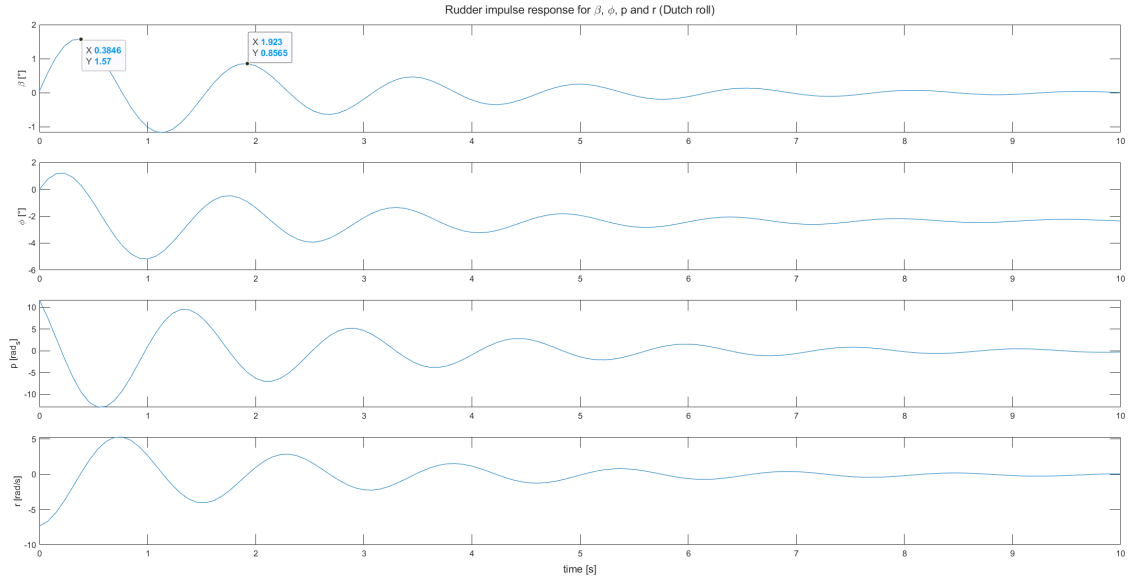

Figure 3.3: Response of sideslip angle, roll angle, roll rate and yaw rate to rudder impulse input (Dutch roll)

4. Design of a pitch rate command system

In this section, a pitch rate command system is being designed. Pitch rate system is effective for tracking tasks at low velocities. The pitch controller has to fulfil the CAP (Control Anticipation Parameter) criterion and and the Gibson criterion.The altitude that has been used in this section is 20000 ft and the velocity is 900 ft/s.

4.1. Short period reduced model

A short period reduced model has only two states, angle of attack α and pitch rate q. The reduced model has been obtained by extracting the $([3,4],[3,4])$ row and column of $A_{Longitudinal}$, $([3,4],[2])$ row and column of $B_{Longitudinal}$, $([3,4],[3,4])$ row and column of $C_{Longitudinal}$, and $([3,4],[2])$ of $D_{Longitudinal}$. The state space model is:

$$\dot{x} = \begin{bmatrix} -0.9748 & 0.9509 \\ -4.276 & -1.317 \end{bmatrix} \cdot \begin{bmatrix} \alpha \\ q \end{bmatrix} + \begin{bmatrix} -0.00205 \\ -0.3139 \end{bmatrix} \cdot \begin{bmatrix} \delta_T \\ \delta_e \end{bmatrix} \tag{4.1}$$

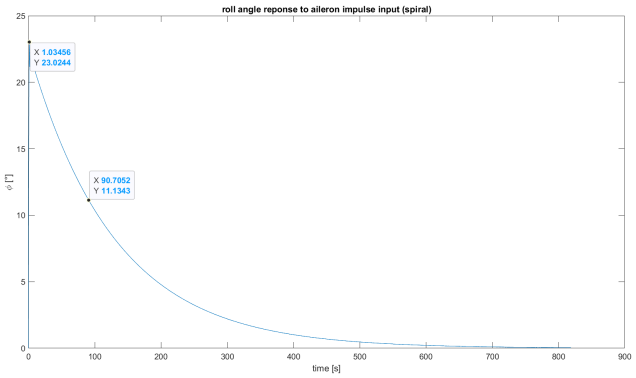

Figure 3.4: Roll angle impulse response to aileron (Spiral)

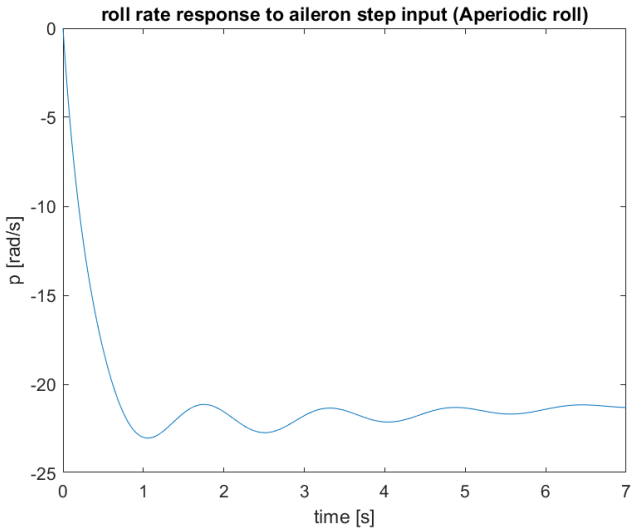

Figure 3.5: Roll rate response to aileron step input (Aperiodic roll)

$$y = \begin{bmatrix} 57.3 & 0 \\ 0 & 57.3 \end{bmatrix} \cdot \begin{bmatrix} \alpha \\ q \end{bmatrix} + \begin{bmatrix} 0 \\ 0 \end{bmatrix} \cdot \begin{bmatrix} \delta_T \\ \delta_e \end{bmatrix} \tag{4.2}$$

$A_{shortperiod}$, $B_{shortperiod}$, $C_{shortperiod}$ and $D_{shortperiod}$ are then shown below:

$$A_{shortperiod} = \begin{bmatrix} -0.9748 & 0.9509 \\ -4.276 & -1.317 \end{bmatrix} \tag{4.3}$$

$$B_{shortperiod} = \begin{bmatrix} -0.00205 \\ -0.3139 \end{bmatrix} \tag{4.4}$$

$$C_{shortperiod} = \begin{bmatrix} 57.3 & 0 \\ 0 & 57.3 \end{bmatrix} \tag{4.5}$$

$$D_{shortperiod} = \begin{bmatrix} 0 \\ 0 \end{bmatrix} \tag{4.6}$$

The 4 states model has been obtained from the previous chapter. The step response of the 2 states and 4 states models is shown in figure 4.1 and figure 4.2. It can be seen that both models show the same behaviour for the first 4 seconds. However, the 2 states model shows a stabilised behaviour after approximately 5 seconds, while the Phugoid motion takeover in the 4 states model. The reason behind is that the 4 states model has the velocity and pitch attitude in it, while the 2 states model does not include the velocity and pitch attitude. The 2 states model can only be used for the designing purposes only for the first 4 seconds since it shows the same behaviour as the 4 states model.

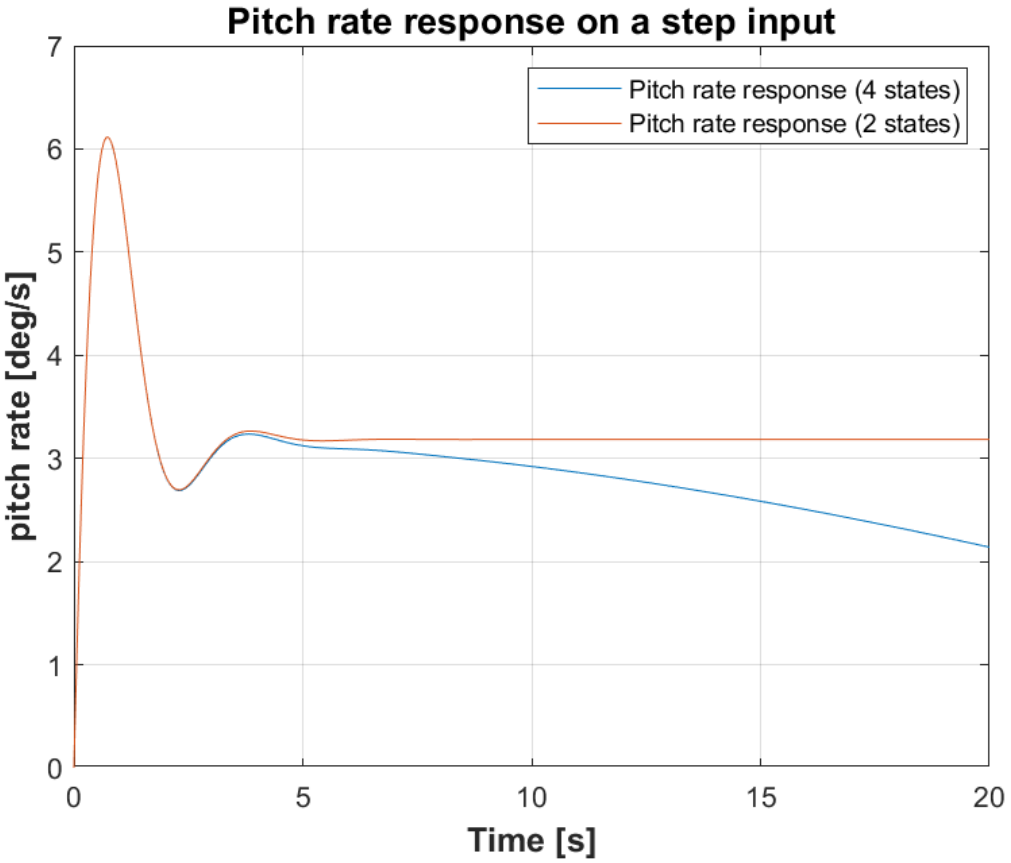

Figure 4.1: Pitch rate q response on a step input for 2 states and 4 states

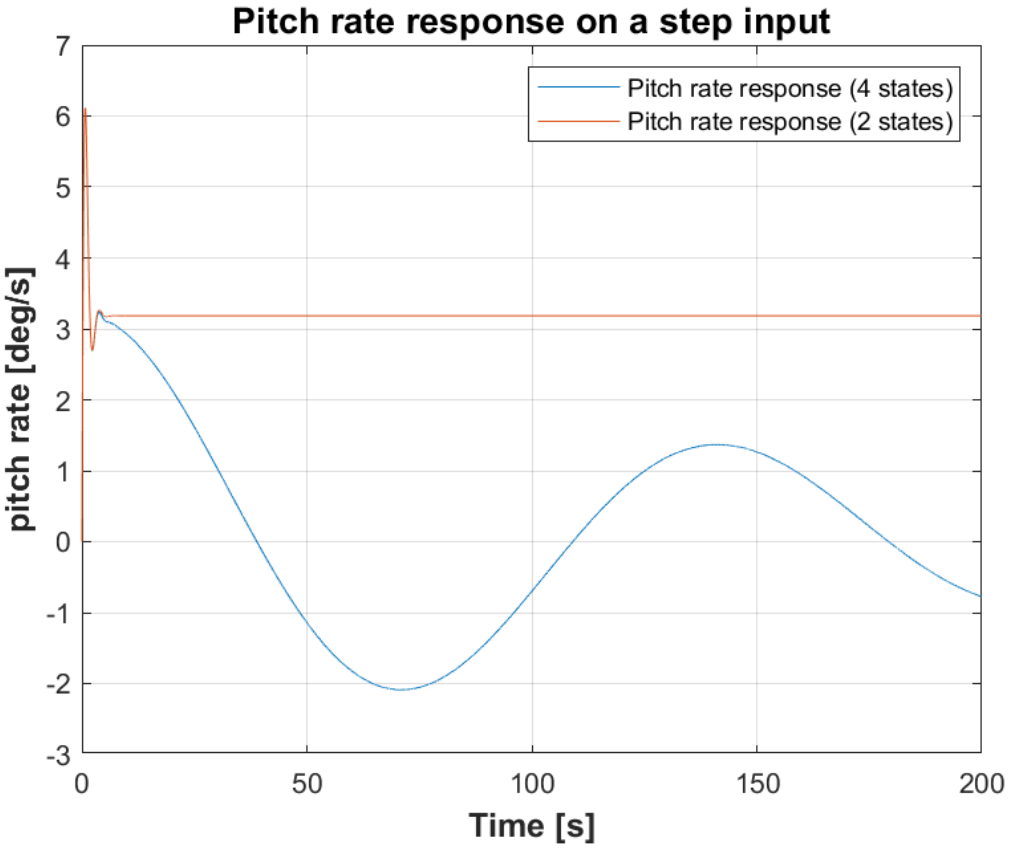

Figure 4.2: Pitch rate q response on a step input for 2 states and 4 states, longer time

4.2. Requirements of the CAP and Gibson criteria and pole placement

Since the requirements of the CAP and Gibson criteria given in the frequency domain (natural frequency $\omega_{n_{sp}}$, damping ratio ζ and time constant $T_{\theta 2}$ are:

$$\omega_{n_{sp}}(V,h) = 0.03V(V,h) \tag{4.7}$$

$$1/T_{\theta 2}(V,h) = 0.75\omega_{n_{sp}}(V,h) \tag{4.8}$$

$$\zeta_{sp}(V,h) = 0.5 \tag{4.9}$$

Solving these equations for the given flight condition of V = 274.32 m/s (900 ft/s) gives:

$$\omega_{n_{sp}} = 8.2296 rad/s \tag{4.10}$$

$$T_{\theta 2} = 0.1620 s \tag{4.11}$$

To obtain the required natural frequency $\omega_{n_{sp}}$ and damping ratio ζ, the below quadratic equation need to be solved in order to determine the position of the poles:

$$s^2 + 2\omega_{n_{sp}}\zeta s + \omega_{n_{sp}}^2 = 0 \tag{4.12}$$

The position of the poles will then be:

$$p_1 = \omega_{n_{sp}}\zeta + \omega_{n_{sp}}\sqrt{\zeta^2 - 1} = 4.1148 + 7.1270i \tag{4.13}$$

$$p_2 = \omega_{n_{sp}}\zeta - \omega_{n_{sp}}\sqrt{\zeta^2 - 1} = 4.1148 - 7.1270i \tag{4.14}$$

The real part of the poles should be in the left hand side to make the system stable, thus:

$$p_1 = -4.1148 + 7.1270i \tag{4.15}$$

$$p_2 = -4.1148 - 7.1270i \tag{4.16}$$

The poles are being placed at these location using the "place" function in Matlab. This procedure gives feedback gains of:

$$K_\alpha = -189.7413°/rad \tag{4.17}$$

$$K_q = -17.6758°/(rad/s) \tag{4.18}$$

To check if the feedback gains are acceptable, severe gust of (design vertical gust: 4.572 m/s) is being considered, with velocity of 274.32 m/s from the flight condition:

$$\alpha_{induced} = \tan^{-1}\frac{V_{gust}}{V} = 0.0167 rad = 0.957° \tag{4.19}$$

$$\delta_c = K_\alpha \alpha_{induced} = -3.1621° \tag{4.20}$$

δ_c is less than 25 °. Thus, it is acceptable.

4.3. Lead-Lag filter

The time constant T_{θ_2} is modified through a pre-filter located outside the loop, because the pre-filter affects and modify the closed loop directly, while if we apply a forward path or feedback compensation that will modify the closed loop transfer function and will create unwanted poles. Thus, the system will be disturbed. Therefore, a lead-lag pre-filter needs to be used:

$$H_{filter} = \frac{1 + T_{\theta_{2new}} s}{1 + T_{\theta_{2old}} s} \tag{4.21}$$

The reduced pitch rate to elevator transfer function is calculated from:

$$\frac{q(s)}{\delta_{el}(s)} = \frac{K_q(1 + T_{\theta_{2old}} s)}{s^2 + 2\zeta_{sp}\omega_{n_{sp}} s + \omega_{n_{sp}}^2} \tag{4.22}$$

The pitch rate to elevator transfer function becomes:

$$\frac{q(s)}{\delta_{el}(s)} = \frac{-2.864s - 17.68}{s^2 + 8.23s + 67.73} \tag{4.23}$$

4.4. Verification of CAP and Gibson criteria

To verify if the system have met the CAP and Gibson Criteria, these following definitions have been implemented:

$$CAP = \frac{\omega_{n_{sp}^2}}{\frac{V}{T}\frac{1}{T_{\theta_2}}} \tag{4.24}$$

$$\frac{DB}{q_{ss}} = T_{\theta_s} - \frac{2\zeta_{sp}}{\omega_{n_{sp}}} \tag{4.25}$$

We obtain values of:

$$CAP = 0.3924 \tag{4.26}$$

$$\frac{DB}{q_{ss}} = 0.0405 \tag{4.27}$$

Pitch rate tracking response, pitch angle tracking response, and Gibson criterion graphs are given figures 4.3, 4.4 and 4.5 respectively: From 4.5, it can be seen that the drop back rate is within the satisfactory limits.

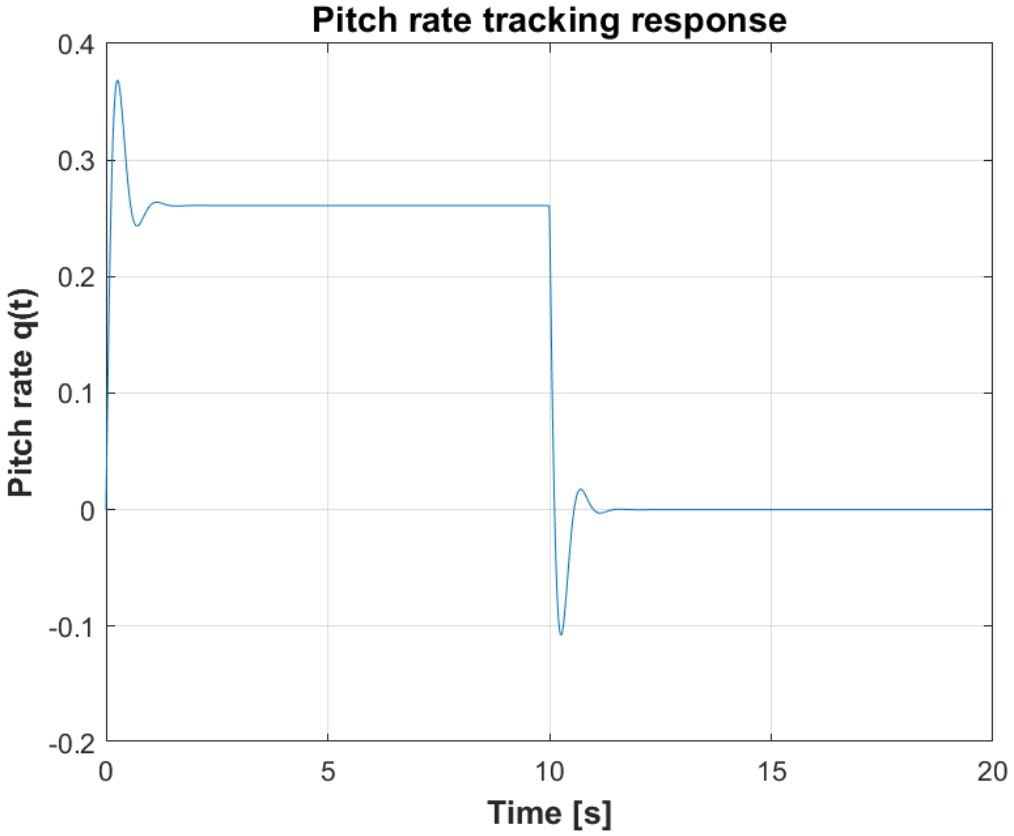

Figure 4.3: Pitch rate tracking response to a step input

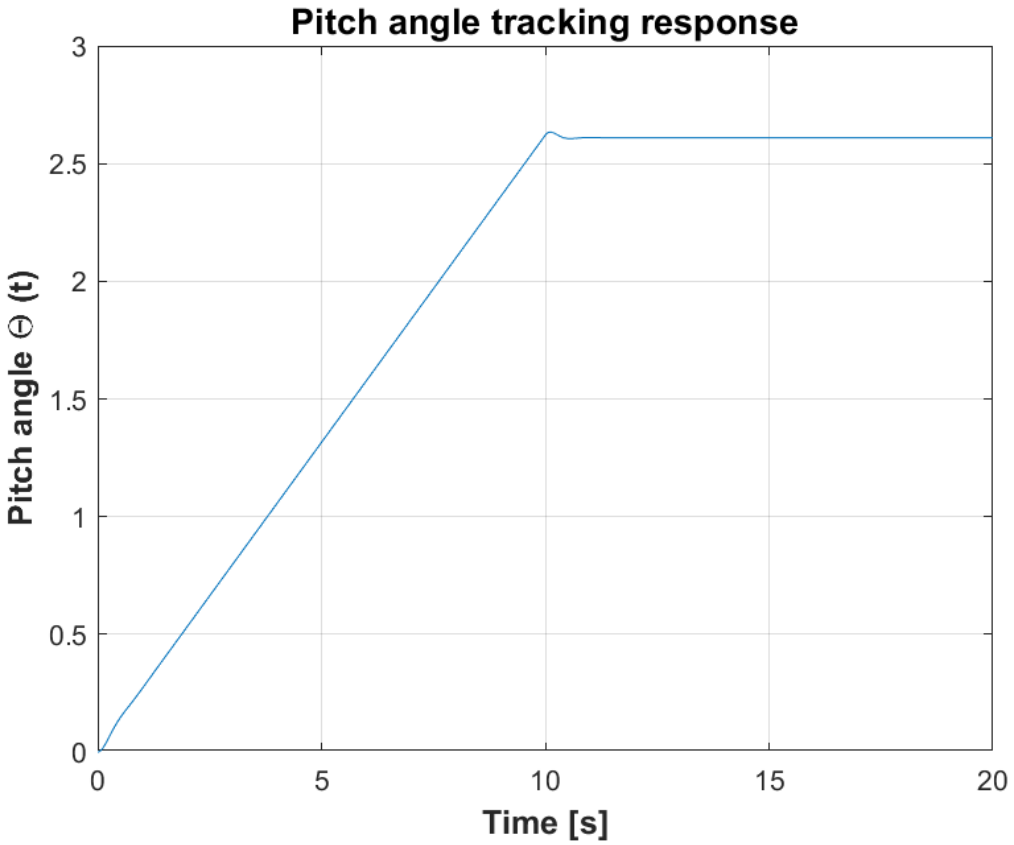

Figure 4.4: Pitch angle tracking response to a step input

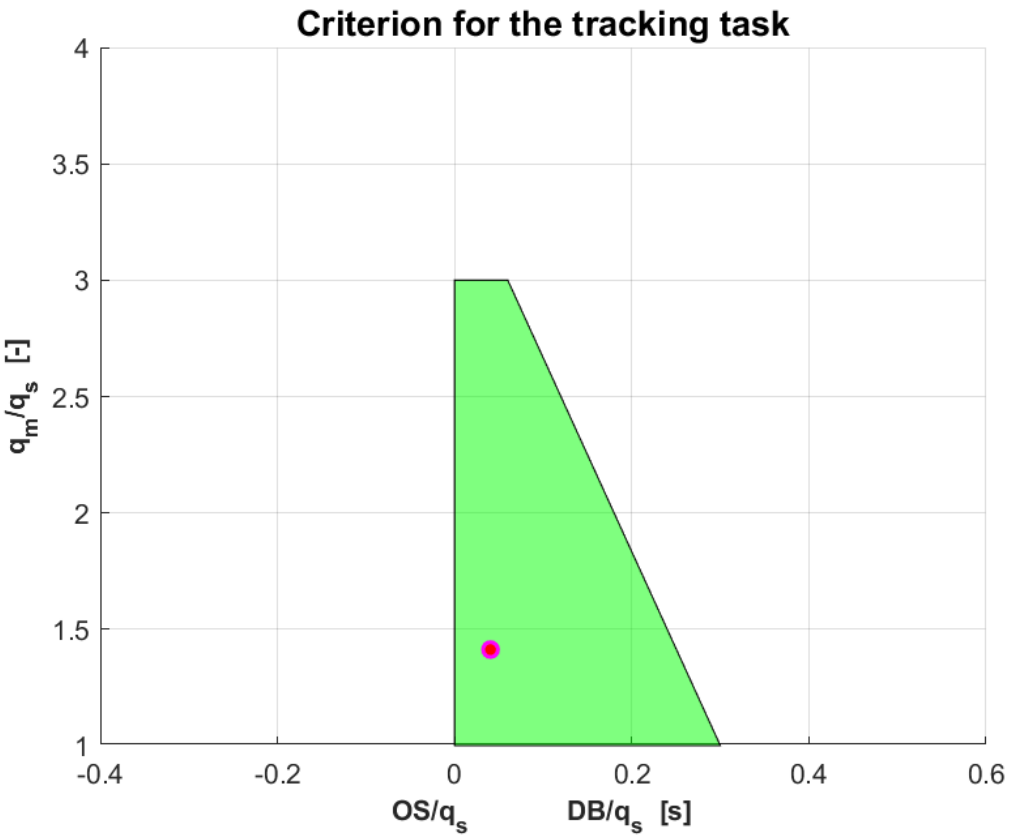

Figure 4.5: Criterion for the tracking response for the reduced model

4.5. Gain Scheduling

The same procedure has been done to the same altitude, but different velocity. Altitude of 20000 ft and velocity of 600 ft/s. Linear interpolation is being used in order obtain a gain scheduling that is valid across this part of envelope.

$$K_q = K_{q1} + (V - V_1)\frac{K_{q2} - K_{q1}}{V_2 - V1} \tag{4.28}$$

Choosing a velocity in between 900 ft/s and 600 ft/s, for example velocity of 700 ft/s. We see from figure 4.6 that it satisfies the drop back criterion as well and within the satisfactory limits.

5. Design of automatic glideslope following and flare controller

5.1. Trimming and linearisation

For this chapter, trimming and linearising is done at an altitude of 5000 ft and with a velocity of 300 ft/s, with a trimming cost of 4.7464e-30 as can be seen in table 2.2.

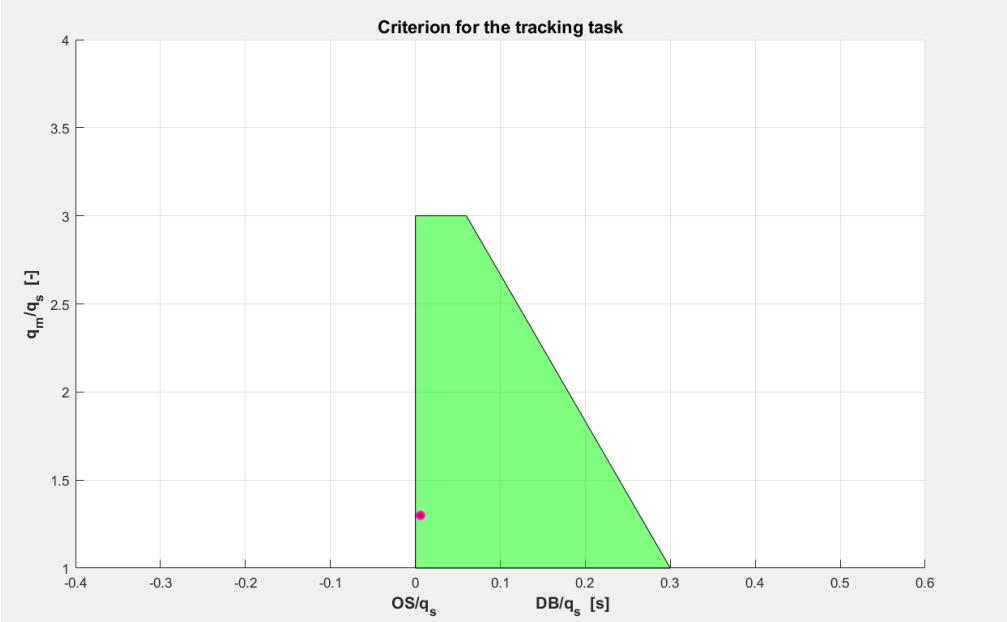

Figure 4.6: Criterion for the tracking response for the reduced model using interpolation

5.2. Reduced model

The reduced model is obtained in a similar way as mentioned in section 3.2, only now containing 5 states: h, V, α, θ, q. The resulting state space system then becomes:

$$\dot{x}_{lon} = \begin{pmatrix} 0 & 0 & -300.0 & 300.0 & 0 \\ 0.00013165 & -0.029097 & 2.13 & -32.17 & -2.8952 \\ 3.1537e-6 & -0.000697 & -0.54466 & 4.5498e-13 & 0.91522 \\ 0 & 0 & 0 & 0 & 1.0 \\ -4.6987e-21 & 1.0385e-18 & 0.33032 & 0 & -0.81694 \end{pmatrix} \cdot \begin{pmatrix} h \\ V \\ \alpha \\ \theta \\ q \end{pmatrix} \tag{5.1}$$

$$+ \begin{pmatrix} 0 & 0 \\ -0.0045338 & 0.001544 \\ -0.0011164 & -9.4931e-7 \\ 0 & 0 \\ -0.057016 & 0 \end{pmatrix} \cdot \begin{pmatrix} \delta_{el} \\ \delta_{th} \end{pmatrix} \tag{5.2}$$

$$y_{lon} = \begin{pmatrix} 1.0 & 0 & 0 & 0 & 0 \\ 0 & 1.0 & 0 & 0 & 0 \\ 0 & 0 & 57.296 & 0 & 0 \\ 0 & 0 & 0 & 57.296 & 0 \\ 0 & 0 & 0 & 0 & 57.296 \end{pmatrix} \cdot \begin{pmatrix} h \\ V \\ \alpha \\ \theta \\ q \end{pmatrix} + \begin{pmatrix} 0 & 0 \\ 0 & 0 \\ 0 & 0 \\ 0 & 0 \\ 0 & 0 \end{pmatrix} \cdot \begin{pmatrix} \delta_{el} \\ \delta_{th} \end{pmatrix} \tag{5.3}$$

5.3. Aircraft model

The aircraft model was equipped with a pitch damper, pitch attitude hold mode and airspeed hold mode. All necessary parameters were tuned using the PID tuner application using a parallel form PID, resulting in the values depicted in table 5.1 In addition, the trim values for the relevant aircraft states were added where necessary to reflect the true values of these states. Caution was taken with the angle units (degrees or radians) to ensure proper functionality. The saturation limits on the elevator and engine setting were implemented as well. The resulting aircraft Simulink model can be found in appendix A.

Controller	PID values (parallel form)
Pitch damper	P = -0.0635335950698202
Pitch attitude hold mode	P = 0.126869189059665 I = 5.34397207151188e-07 D = 3191.97869211359
Airspeed hold mode	P = 100.544379315609 I = 6.08761343845027 D = -35.7772852997847

Table 5.1: Tuning values cor aircraft control loops

5.4. Airfield module and glide slope controller

In order to design the glide slope controller, certain values need to be known to the aircraft in reference to the airport, the most important of which is the glide slope error angle Γ. Note that in reality, the airfield broadcasts radio frequencies in order for the aircraft to determine its glide slope angle. In this context however, a virtual model is made using exact values that are known to the simulation environment.

5.4.1. Airfield: Glide slope error angle and slant range

The following graphical representation defines the reasoning for the design layout and calculations:

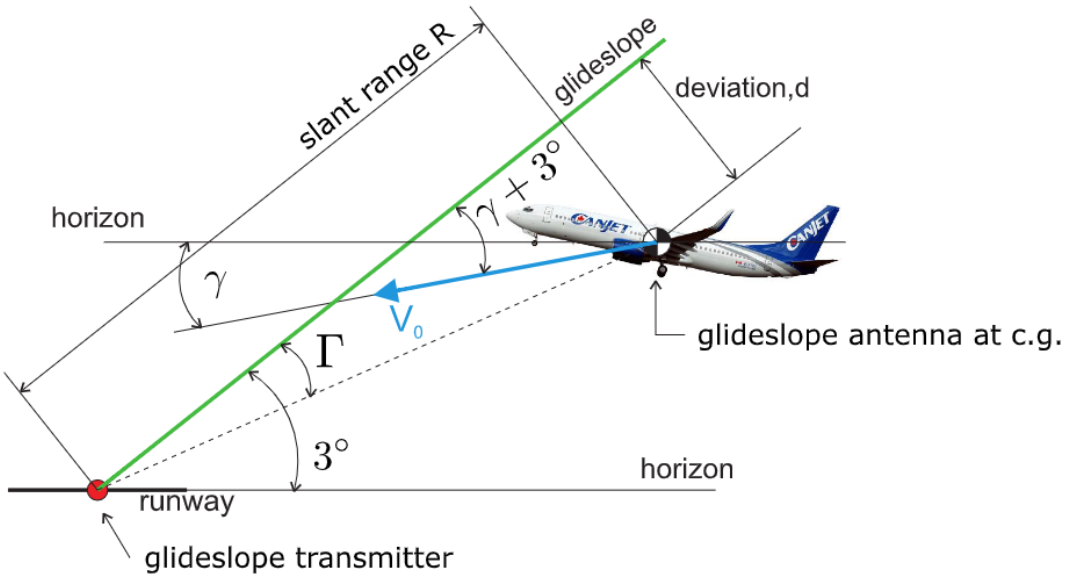

Figure 5.1: Graphical representation of the glide slope

From the aircraft model, the following parameters can be used: Altitude (h), Velocity (V), and the aircraft glide slope (γ). In order to calculate Γ and the slant range R (note that the slant range was only used to verify the workings of the model):

Glide slope error angle Γ:
Define

$$\beta = 3° - \Gamma \tag{5.4}$$

And

$$3° = \Gamma + \beta \tag{5.5}$$

$$\beta = \arctan\frac{h}{x} \tag{5.6}$$

Then

$$\Gamma = 3° - \arctan\frac{h}{x} \tag{5.7}$$

Slant range R:

$$R = \frac{d}{\Gamma} = \frac{d}{3° - \arctan\frac{h}{x}} \tag{5.8}$$

With

$$d(s) = \frac{V_0}{s}(\gamma + \frac{3\pi}{180}) \tag{5.9}$$

Note that h is known and the horizontal distance x can be calculated according to the desired reference (as we know the glide slope γ and the aircraft velocity V). The airfield module block diagram can be found under Appendix C

5.4.2. Glide slope controller

For the horizontal distance x, the reference point x_0 is set to be 3000ft., as the requirement is that the glide slope is intercepted after 10 seconds (and the speed is maintained at 300 ft/s). The model has been programmed in such a way that the θ reference that is being fed back into the aircraft model is calculated by the glide slope coupler. The altitude that is being flown towards is 3000ft. (airfield pressure altitude), meaning ±3000ft. on the aircraft altimeter implies touchdown.
The glide slope coupler uses the glide slope error angle Γ as input and calculates the corresponding θ reference that becomes the input for the aircraft model (after interception). The transfer function of the coupler:

$$H_{coupler} = K_c(1 + \frac{W_1}{s}) \tag{5.10}$$

It was chosen to take $W_1 = 0.1$ and $K_c = 50$ as this gave the smoothest results. The following graph clearly shows the path of the aircraft and interception point of the glide slope. The angle formed is indeed 3° (note that the X and Y axis are not for scale for demonstration reasons):

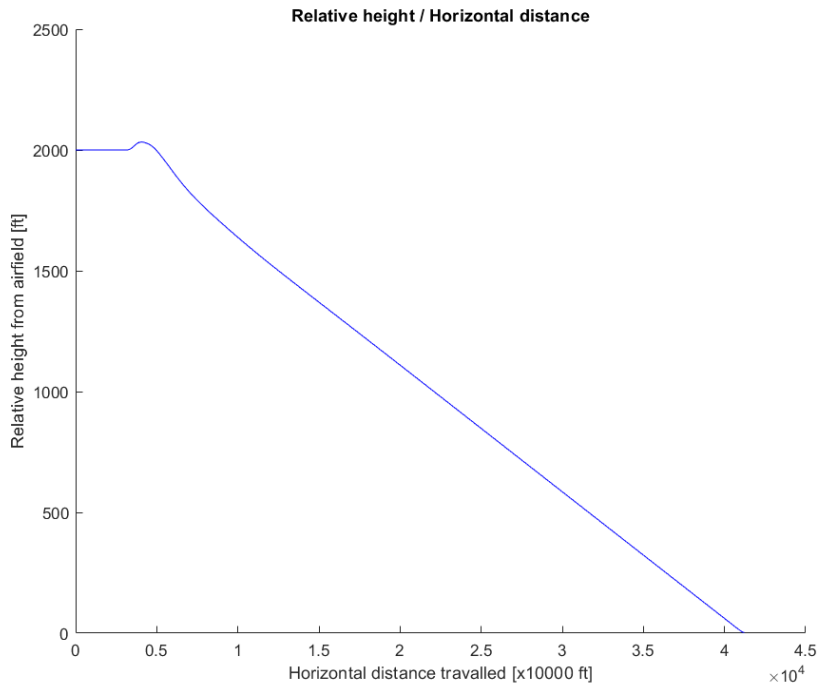

Figure 5.2: Aircraft path relative to airport altitude

The glide sloper coupler, as well as the complete system block diagram (and therefore links needed for the glide sloper controller) can be found under Appendix D and E, respectively.

5.5. Flare controller

The flare controller consists of a coupler, and inputs from the aircraft model that consist of altitude, glideslope, velocity, and reference altitude that is considered 0. The output of the controller is θ_{ref}. The coupler is PI a controller:

$$H_{coupler} = K_c(1 + \frac{W_1}{s}) \tag{5.11}$$

For which the value of K_c is chosen to be 50 and the value of W_1 to be 0.1. It is assumed that during flare that the ground speed is kept constant at 300ft/s and that the vertical speed at touchdown is 3 ft/s. The geometry of the flare can be seen in figure 5.3. It is also assumed that the flare controller will take over at a height of 14 ft. The Simulink model of the flare controller can be seen in appendix B. The resulting flare manoeuvre can be seen in figure 5.4. It should be noted that the upward motion after the flare is due to simulation time being extended after touchdown.

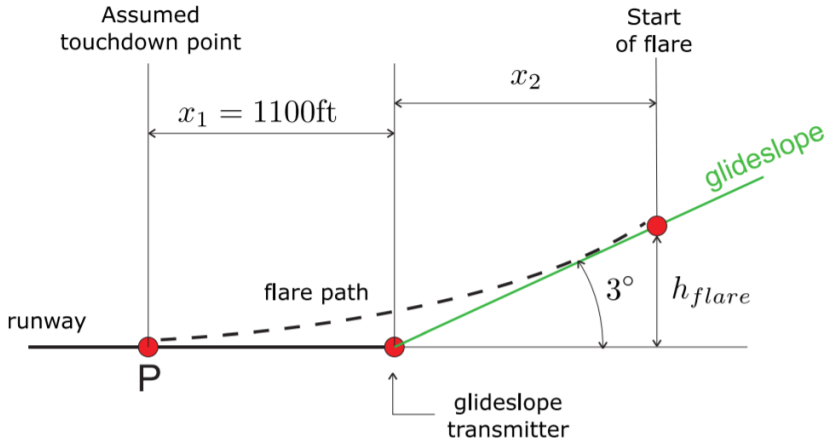

Figure 5.3: Flare Controller Geometry

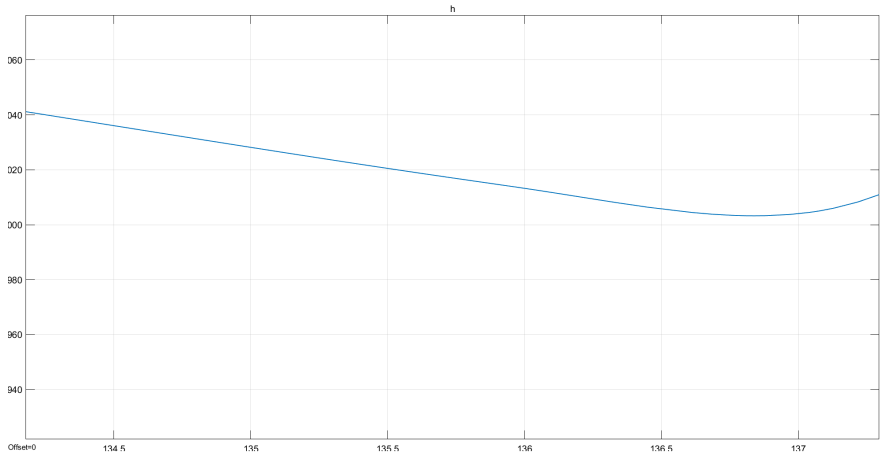

Figure 5.4: Flare manoeuvre

A. AIRCRAFT SIMULINK MODEL

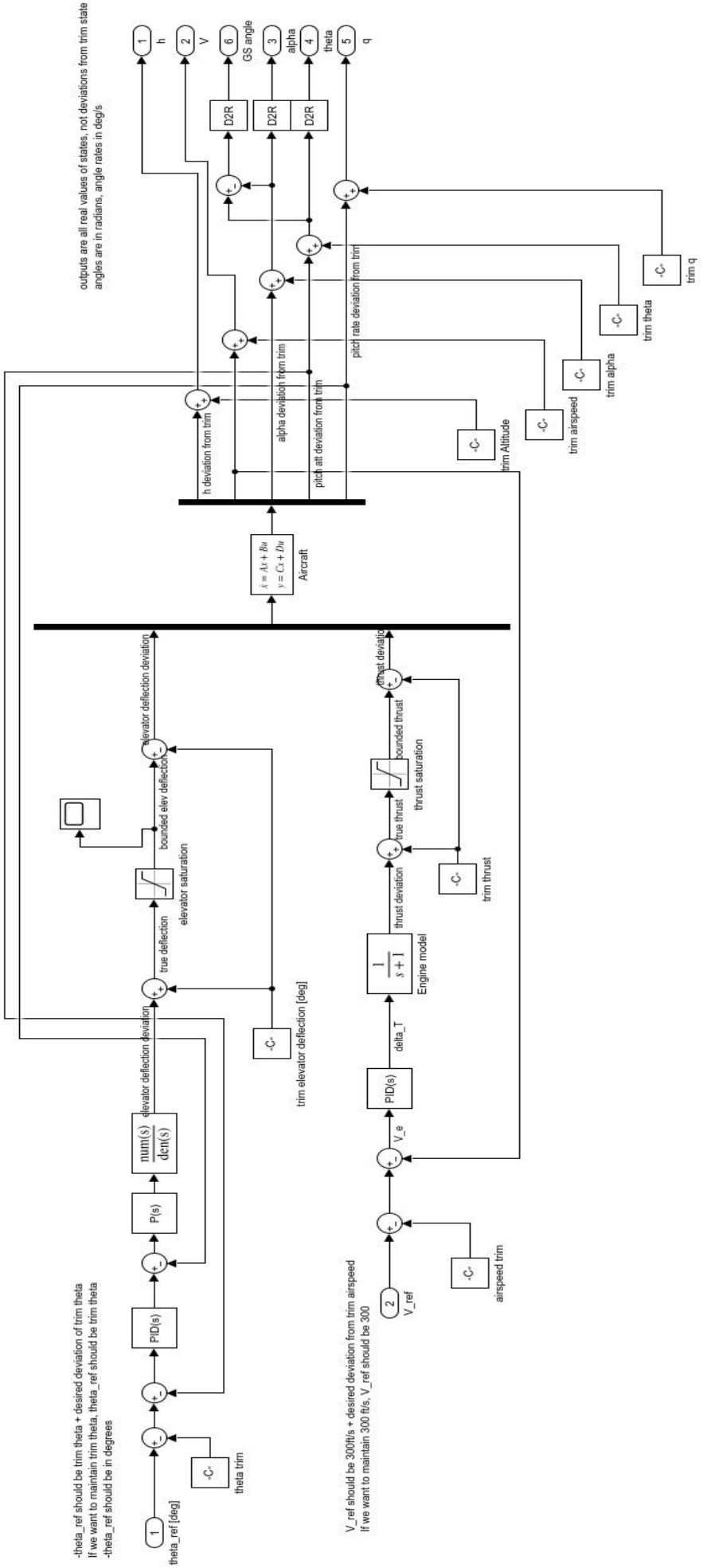

B. FLARE CONTROLLER SIMULINK MODEL

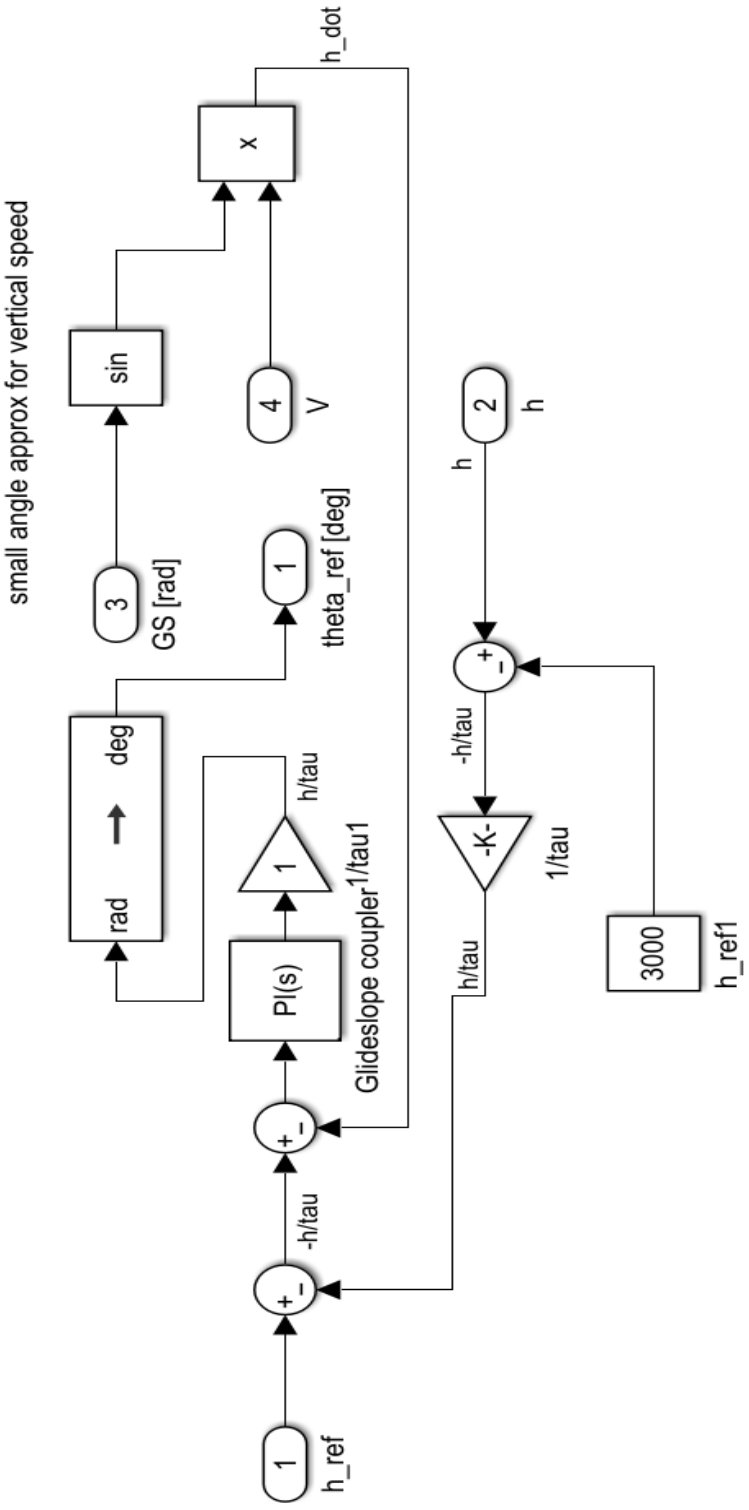

C. AIRFIELD MODULE

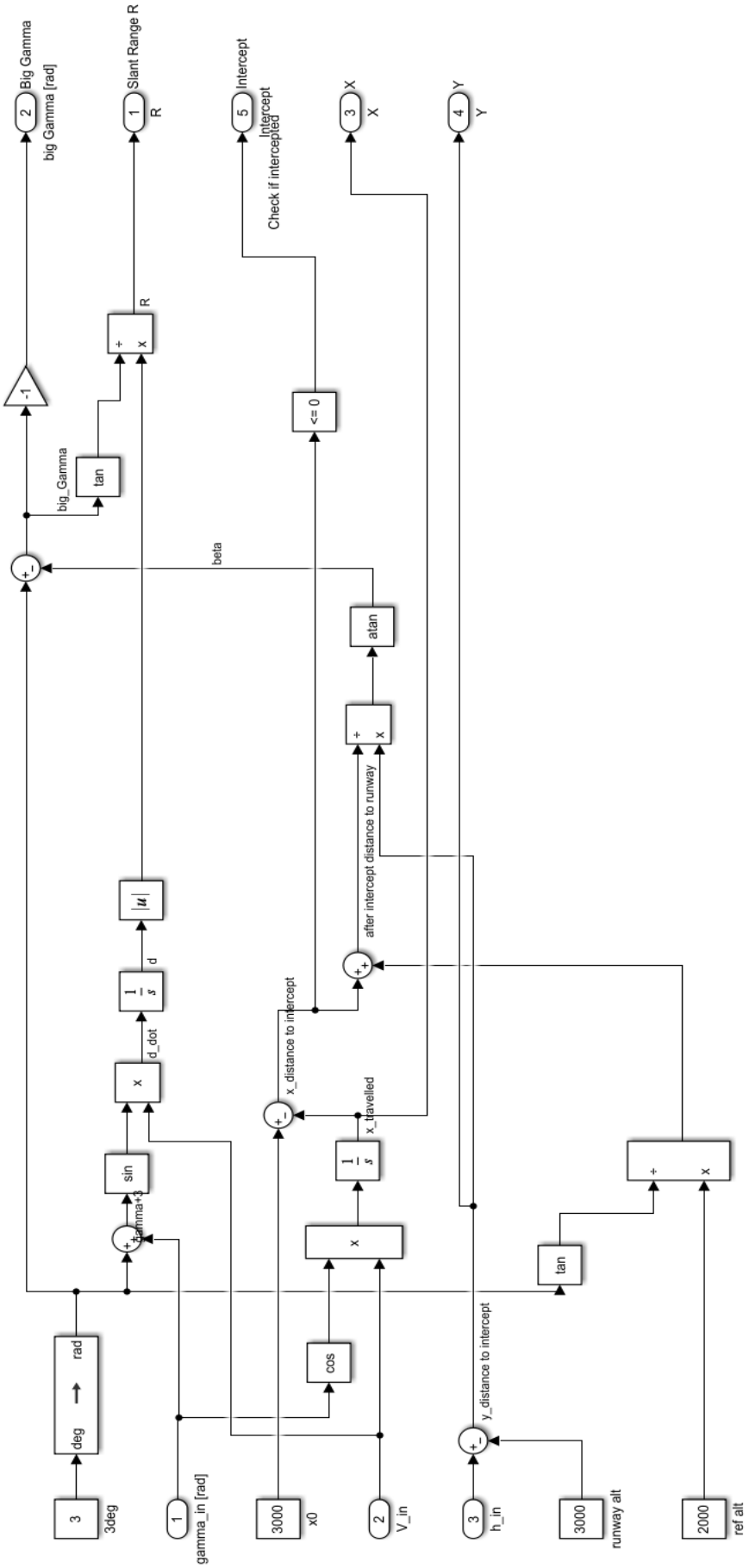

D. GLIDE SLOPE COUPLER

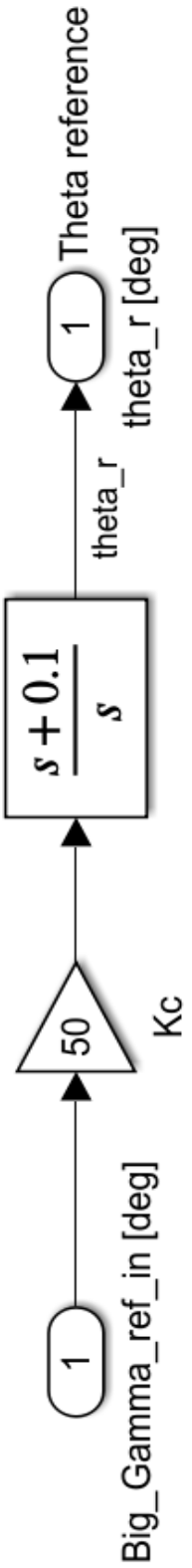

E. COMPLETE SYSTEM